IEEE Access
Multidisciplinary ⁝ Rapid Review ⁝ Open Access Journal

Received January 15, 2020, accepted February 10, 2020, date of publication February 18, 2020, date of current version March 2, 2020.

Digital Object Identifier 10.1109/ACCESS.2020.2974885

A Deep Adaptive Traffic Signal Controller With Long-Term Planning Horizon and Spatial-Temporal State Definition Under Dynamic Traffic Fluctuations

SHURONG LI, CHONG WEI, XUEDONG YAN, LU MA, DEQI CHEN, AND YING WANG
MOT Key Laboratory of Transport Industry of Big Data Application Technologies for Comprehensive Transport, School of Traffic and Transportation, Beijing Jiaotong University, Beijing 100044, China

Corresponding authors: Chong Wei (chwei@bjtu.edu.cn) and Lu Ma (lma@bjtu.edu.cn)

This work was supported in part by the Fundamental Research Funds for the Central Universities under Grant 2019JBM040, and in part by the National Natural Science Foundation of China under Grant 71971017, Grant 91746201, and Grant 71621001.

ABSTRACT This study proposes a new adaptive traffic signal control scheme to effectively manage dynamically fluctuating traffic flows through intersections. A spatial-temporal representation of the traffic state at an intersection has been designed to efficiently identify traffic patterns from complex intersection environments, and a deep neural network (long short-term memory network, LSTM) is used to determine look-ahead signal control decisions based on the estimated long-term feedback from a given traffic state. The actor-critic algorithm, one of the reinforcement learning-based algorithms, is adopted to obtain the essential parameters of the LSTM deep neural network through multiple interactions between a simulated environment and the corresponding adaptive traffic signal controller. A realistic model environment comprising a 24-hour time-varying traffic demand including rush hour and non-rush hour situations served as the basis for traffic generation in the numerical experiments to confirm the effectiveness of the proposed scheme. The results of these experiments show that, compared to an optimized fixed time plan (Synchro), the proposed scheme can reduce waiting times at intersections by an astounding 50% with consequential benefits of reducing fuel consumptions, emissions, queue lengths, and vehicle delays whilst increasing mean speeds.

INDEX TERMS Adaptive traffic signal control, reinforcement learning, spatial-temporal traffic state representation, actor-critic, LSTM, 24-hour dynamic traffic fluctuations.

I. INTRODUCTION

It is generally accepted that the efficient management of traffic flows to reduce travel delay, especially through intersections, is an essential objective in traffic management. Attempting to achieve this objective is Adaptive Traffic Control which has an advantage in that it can take real-time and stochastic traffic demand into consideration and provide traffic light control decisions based on a wide range of algorithmic designs including dynamic programming, fuzzy logic and reinforcement learning as reported in various studies [1]–[5]. However, based on an examination of these previous studies, it is clear that the design of an adaptive traffic control algorithm is plagued by three crucial problems outlined as follows:

Firstly, an effective method is needed to represent, as accurately as practically possible, the time-varying traffic flow situation (usually referred to as the traffic state) at a target intersection to include additional operating information pertinent to the particular intersection [5]. In such a method, in order to maintain accuracy or rather preserve as much information as possible, it would seemingly be convenient to use an approach based on microscopic measures (such as the position and velocity) of individual vehicles rather than macroscopic measures (such as traffic flow). However, as an intersection is a complex system involving the positions and velocity profiles of multiple vehicles, such an approach can be adversely impacted by high computation costs (the curse of dimensionality), which in previous studies were avoided

The associate editor coordinating the review of this manuscript and approving it for publication was Sabah Mohammed.

through the use of aggregate (macroscopic) measures such as flow rate, flow speed and vehicle queue length instead of the individual (microscopic) measures of vehicle positions and velocities to represent the traffic state [3], [6], [7]. Although these aggregate measures simplify traffic state representation, specific vehicular information at a target intersection is inevitably lost. On the other hand, even if individual vehicle positions and velocities are considered, delay information is lacking for each vehicle as well as for the intersection system resulting in the inability to effectively minimize the total delay for each traffic light control decision.

Secondly, although in recent years a considerable number of studies have employed macroscopic traffic flows in their underlying traffic flow models, there remains a problem in that these models cannot precisely reflect the actual traffic flow characteristics of a target intersection which negatively impacts evaluating the real-time performance of control policies in adaptive traffic signal control algorithms [8]–[11]. As already mentioned in the statement of the first problem, there is good reason for using macroscopic traffic flow models in that their computational costs are relatively low, so they can easily be implemented in adaptive control algorithms. This computational benefit was a contributary factor which effectively led to the implementation of some well-known adaptive traffic control systems, such as SCOOT [12], SCATS [13] and COP [14]. However, there still remains the problem that macroscopic traffic flow models cannot precisely reflect the traffic flow characteristics of a target intersection.

The third problem relates to the modelling of traffic demand at an intersection, which normally involves using vehicle arrival rates as the basis for such modelling. However, previous studies mainly assume that the arrival rate is constant throughout the day [3], [7], [15], [16], treating rush hour and non-rush hour traffic as the same homogeneous conditions. Clearly, this assumption can lead to the poor performance of traffic signal control schemes, especially during rush hours. Furthermore, although the Annual Average Daily Traffic (AADT), obtained from historical observation data, is used to provide aggregate information for traffic signal control, we found that few algorithms can exactly take into account the 24-hour time-varying traffic demands, arguably needed to further enhance the design of traffic signal control schemes.

Addressing these three problems, the research underpinning this study establishes a fundamental decision-making framework which uses a Reinforcement Learning (RL) approach supported by a deep neural network to implement an adaptive traffic control algorithm [17], [18]. The main reason behind this approach is the recognition that RL has recently contributed to effective decision-making in several other areas such as gaming and robotics, as well as in traffic control [19]–[24]. Furthermore, previous studies have confirmed that RL can effectively work with microscopic traffic flow models for adaptive traffic control and can make look-ahead control decisions for an intersection system [4], [25].

This study focuses on reducing the total delay of vehicles through the design of a signal controller that can identify both the spatial and temporal patterns in real-time traffic based on microscopic information so as to reduce information loss. To reflect spatial traffic situations as realistically as possible, individual vehicle delays are defined as the basic element of the traffic state, and an intersection is partitioned into cells that represent individual delays. Moreover, to capture the temporal traffic dynamics, we employ a series of spatial observations to enhance the representation of the traffic state, which is then used as input into a neural network to determine the control decisions at different time intervals. Note that the type of neural network used in this study is the LSTM network because it is especially suited to time sequence problem modelling. This type of network, therefore, provides the essential basis for dealing with complex traffic states as represented by microscopic vehicular and other operational information without suffering from the curse of dimensionality [26], [27]. The proposed adaptive signal controller enables control decisions based on the guidance of the trained neural network after it has learnt an optimal control policy through multiple trial-and-error interactions between the controller and the intersection environment.

Reinforcement learning (RL) is employed to determine the parameters of the LSTM network under a microscopic traffic simulation environment given dynamic traffic demand scenarios [28]. It should be noted that in previous studies, traffic demand scenarios for training procedures were usually generated assuming a constant vehicle arrival rate [7], [15], [16]. In this study, however, vehicle arrivals are generated following a Poisson distribution for a 24-hour time-varying traffic demand curve obtained from historical data. This method allows the training procedure to take into account daily traffic dynamics and reflects the stochastic nature of traffic demand.

To ensure the convergence of the RL algorithm, we employed an actor-critic strategy in the RL model to optimize the parameters of the LSTM network. Moreover, we used multistep bootstrapping technique and clipped surrogate objective technique to enhance the algorithm efficiency and robustness. We finally provide a framework for the RL that is specially designed for adaptive traffic control. The contribution of this paper can be concluded as follows:

Firstly, in previous RL studies, the consideration of individual vehicular delay information for processing by traffic controllers was usually ignored. Addressing this omission, we propose a novel traffic state definition to identify both the spatial and temporal patterns using microscopic traffic delay information. This method reduces information loss and provides individual vehicular delay information for each traffic light control decision.

Secondly, we have designed a RL algorithm framework to determine the parameters of the LSTM network in a microscopic simulation environment. This framework can guarantee the convergence of the learning process under complex traffic states.

Thirdly, the RL algorithm executes the learning process based on a 24-hour time-varying traffic demand, which incorporates both rush hour and non-rush hour situations. This enables realistic observations of commuting traffic in practice and can provide substantial practical benefits in the implementation of adaptive traffic control.

Following on from this introduction, the remainder of this paper is arranged as follows: Section II presents a literature review. Section III provides background information for the traffic signal control scheme, involving delay, cost and state. In Section IV, we describe the optimization algorithm, an actor-critic algorithm combined with a multistep bootstrapping technique and a clipped surrogate objective technique. In Section V, we describe the setup of the numerical experiment and present the results to demonstrate the performance of the proposed method. In Section VI, we conclude our work on the proposed method and provide some suggestions for future work.

II. LITERATURE REVIEW

There are currently two basic types of traffic signal control: fixed-time signal control and adaptive signal control. In the case of fixed-time control, the controller utilizes historical traffic data to determine signal timing off-line [29]. Fixed-time control has been widely used in several well-known signal timing systems, such as the TRANSYT [30], SYNCHRO [31] and MAXBAND [32] systems. Fixed-time control performs stably if the traffic demand follows a fixed pattern; however, it cannot respond to stochastic traffic conditions, especially in situations where there is a sudden buildup of traffic.

Adaptive signal control utilizes real-time data to determine an optimal signal timing to maximize a defined objective function and in recent decades it has gradually gained popularity due to its adaptability and flexibility. The controller managing adaptive signal control can be classified according to the type of control it provides, namely: responsive signal control, online optimization control, or revising frequency control [33]. Each of these control classifications is discussed as follows:

A. RESPONSIVE SIGNAL CONTROL

In the case of responsive signal control, each signal in a controller seeks a decision to extend the current green phase or not, based on the upstream actuated traffic demand. A typical signal control system is the modernized optimized vehicle actuation (MOVA) system [34]. However, a disadvantage of this system is that it fails to optimize globally because the control decision only considers the traffic demand in the current green direction whilst ignoring all other directions.

B. ONLINE OPTIMIZATION CONTROL

The online optimization algorithm utilizes model predictive control [35], traffic flow model control [10], [36] and Petri nets model control [37] to make control decisions considering detected and predicted future traffic. Typical existing systems using online optimization include the SCOOT [12] and SCATS [13] systems, which have shown significant improvements in the performance of traffic signal control. However, almost all of these systems were developed using macroscopic traffic flow models, which implies the loss of detailed information about individual vehicle movements at an intersection and, therefore, results in poor performance regarding control decisions.

C. REVISING FREQUENCY CONTROL

The revising frequency control approach uses a rolling horizon and starts an optimization every few seconds to maximize an objective function over the planning period. The main feature of the revising frequency control approach is that the traffic signal timing is optimized at a rather fast pace, and the resolution can be as short as 0.5 seconds [38]. This method makes it possible to control traffic signals effectively in many practical applications, such as the PRODYN [39], OPAC [40], RHODES [41] and COP [14] systems. The techniques used to solve the rolling horizon problems include dynamic planning and reinforcement learning (RL), with the latter technique gaining popularity in recent research because of its computation feasibility and its adaptability in complex problems [38]. Extensive research, therefore, has been conducted in traffic signal control using RL [5]. In one such research, as a pilot study, a multiagent traffic signal control scheme with a model-based RL was developed to minimize the overall waiting time of vehicles. This study confirmed the effectiveness of its RL-based adaptive signal control algorithm through comparing the performance of the RL controller and non-adaptive traffic signal controllers. The author employed Q-learning to minimize the number of waiting vehicles for an isolated intersection with aggregate state information such as the queue length in its four approaches [42]. The advantage of RL in the revising frequency control method was further confirmed through the comparison of RL with function approximation and dynamic planning [38]. RL can be divided into three categories: value-based RL, policy-based RL and actor-critic RL. The author has shown that actor-critic RL, a combination of value-based RL and policy-based RL, outperforms the other two algorithms and has many benefits in terms of robustness, training speed and the generalization of new traffic scenarios [7]. Recent studies have also combined deep neural networks with RL to implement traffic control and have shown that such a combination can significantly improve the robustness and generalization ability of RL [7], [43]. In addition, a deep neural network enables RL to handle higher dimensions of traffic state representations more efficiently including the complex and stochastic characteristics of real-world traffic systems [25].

III. TRAFFIC SIGNAL CONTROL SCHEME

For a typical intersection (Section III-A), the traffic efficiency is largely influenced by the traffic signal control scheme and thus the traffic signal controller plays a critical role in building a safe, efficient, and environmental driving environment

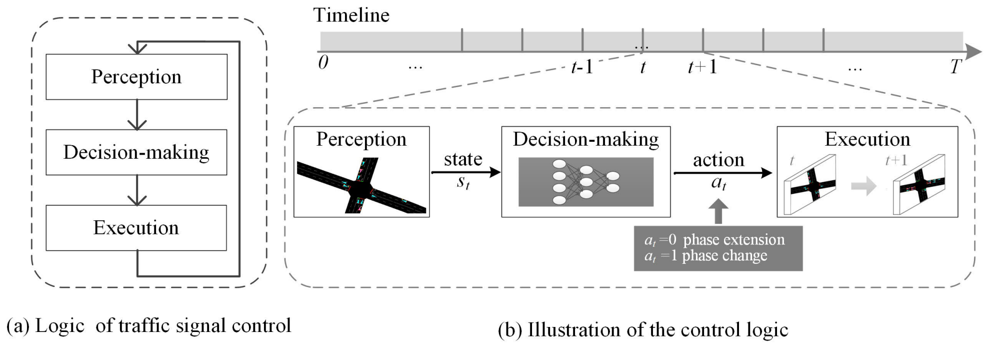

FIGURE 1. Schematic representation of traffic signal control.

in city traffic conditions. In this study, we adopt vehicle delay to evaluate traffic efficiency and construct objective function by minimizing the total delay J of surrounding vehicles at the intersection (as introduced in Section III-B).

Fig. 1 shows the proposed control scheme. We divide the time horizon into several discrete time intervals, and each time interval is indexed by t with a duration of Δt. For each time interval t, the signal control is fullfilled by three stages: perception, decision-making, and execution. In the perception stage: the controller first detects the positions and speeds from surrounding vehicles information at time interval t through several types of smart sensors, such as millimeter-wave traffic radar and computer vision-based traffic monitors; then the controller estimates the state s_t using the method in Section III-C to extract representative information without losing too much information. In the decision-making stage, the controller gives action a_t between two choices: to extend the current phase ($a_t = 0$) or change into the next phase ($a_t = 1$) based on the observed state s_t; the basic logic of this is that a trained neural network function can predict the optimal action a_t using state s_t as input, where its internal parameters are obtained using RL through multiple interactions between the controller and simulation environment (as introduced in Section IV). Finally, in the execution stage, the traffic light will carry out the planned action a_t for Δt (for $a_t = 0$) or $\Delta t_{\text{yellow}} + \Delta t$ (for $a_t = 1$) seconds, observe the control feedback cost j_t and begin the next iteration of time interval $t + 1$.

A. CELL-BASED INTERSECTION LAYOUT

Fig. 2 shows a typical single intersection that has four-direction legs. Each leg consists of multiple approaching links and departure links. We use Ω to denote the approaching link set. Furthermore, we divide each approaching link into multiple cells to collect useful information about the vehicle movements, where the cells are labeled with $0, 1, 2, \ldots, i, \ldots, N_i$. Since the minimum space headway of two successive vehicles is 7.5 m, each cell span 7.5 meters when dividing cells. This can benefit the precise state representation and reduce information loss through a high-resolution space division method.

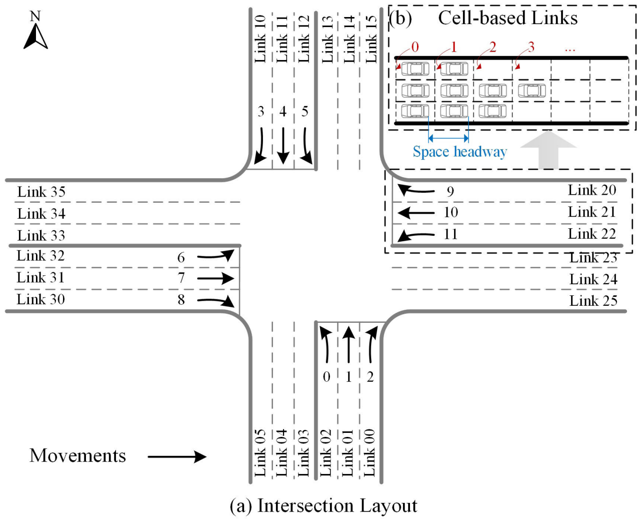

FIGURE 2. Illustration of a typical network.

B. DELAY AND COST FUNCTION

When approaching an intersection, vehicles might slow down as a result of catching up to the vehicles in front or they may have to stop because of a red light. We define the vehicle delay $d_t(k)$ as the amount of extra time for vehicle $k \in U_t$ to at time interval t:

$$d_t(k) = \Delta t(1 - \frac{v_t(k)}{v_{\text{free}}}) \tag{1}$$

where Δt is the duration of time interval t, $v_t(k)$ is the average speed of vehicle k during time interval t, v_{free} is a constant that indicates the speed of a vehicle passing through the intersection under the free-flow conditions and U_t is the set of the vehicles located on the approaching links of the intersection at the beginning of the time interval t. Note that for vehicle k, the average speed $v_t(k)$ is associated with phase decision a_t, and the current state s_t. If the corresponding phase is green, the vehicle might travel with a high speed, however, if the corresponding phase is red, the vehicle should slow down (low speed) and stop.

For each time interval t, the controller's performance can be evaluated by cost j_t:

$$j_t = \sum_{k \in U_t} d_t(k) \tag{2}$$

where cost j_t considers the total delay for surrounding vehicles U_t.

Furthermore, based on the cost of each time interval, the total cost function of the controller can be derived as:

$$\min_{a_t} J = \sum_{t=0}^{T} j_t \tag{3}$$

where T is the total number of time intervals in the planning horizon. Minimizing cost J is consistent with the fact that our controller aims at improving the traffic efficiency by manipulation phase extension or not over the planning horizon $[0, 1, 2, \ldots, T]$.

C. STATE DEFINITION

The traffic controller makes action decisions based on the representative state of the target intersection. We propose a method to collect the multidimensional information to represent the traffic state to reduce the information loss caused by partial observability. In previous works, the traffic state definition is usually simply represented by the aggregate information, such as the average queue length or waiting time of the vehicles located in the intersection. However, such representation ignores individual differences and spatial information. This study proposes a method that can take into account the travel time delay for each vehicle in the intersection and maintain the dimensions of the input as a constant even if the number of vehicles at an intersection is time-dependent.

Since the size of U_t is time-dependent, it is not proper to use $d_t(k)$ directly as the representation of the state. We define delay D_t^i for cell i as follows:

$$D_t^i = \begin{cases} \dfrac{\sum_{k \in U_t^{(i)}} d_t(k)}{|U_t^{(i)}|} & \text{if } |U_t^{(i)}| \neq 0, \\ 0 & \text{if } |U_t^{(i)}| = 0. \end{cases} \tag{4}$$

where U_t^i denotes the set of vehicles that are located at the cell i at time t. If $|U_t^i| = 0$, it means that no vehicle has been checked in cell i at time t and therefore D_t^i is equal to 0. In the case of $|U_t^i| \neq 0$, we use the mean delay value of the vehicles as the delay value of the cell i at time t. We further use D_t to denote the delay information for the intersection as follows:

$$D_t = [D_t^0, D_t^1, \ldots, D_t^i, \ \ldots, D_t^{N_i}] \tag{5}$$

where N_i is the total number of cells at the approaching links for the target intersection. D_t^i can be obtained by observing the speeds of the vehicles in cell i during time interval t. Our proposed method does not require the tracking of the trajectories of each vehicle at an intersection. Therefore, the proposed state representation method is adaptive and easily implemented for several types of smart sensors, such as millimeter-wave traffic radar and computer vision-based traffic monitors.

Furthermore, in order to restrain the phenomenon that the phase keeps fast flip, we use c_t to denote the cumulative repetition number of the current phase until the end of the last time interval $t-1$ which can be expressed as:

$$c_t = \begin{cases} c_{t-1} + 1 & \text{if } a_{t-1} = 0, \\ 0 & \text{if } a_{t-1} = 1. \end{cases} \tag{6}$$

c_t is 0 when the signal controller switches into the next phase ($a_{t-1} = 1$) and $c_t = c_{t-1} + 1$ when the signal controller decides to remain in the current phase ($a_{t-1} = 0$) at the last time interval $t-1$.

In conclusion, we introduce the spatial observation x_t and state s_t definitions to capture the spatial and temporal dynamics in a complex traffic environment.

$$\begin{aligned} x_t &= [\phi_t, c_t, D_t] \\ s_t &= [x_{t-\xi+1}, x_{t-\xi+2}, \ldots, x_t] \end{aligned} \tag{7}$$

where $\phi_t \in \{0, 1, 2, 3\}$ is refered to the traffic signal phase at time t (see Fig. 3). ξ is the number of observed timesteps.

An example is provided to illustrate the evolution of the proposed state representation method. As shown in Fig. 3, the controller executes the signal phase ϕ_t, sequentially from phase 0 to phase 3. The value of ξ is set to 10 for illustration purposes. We assume that time interval $t-1$ begins with phase $\phi_{t-1} = 1$ and phase repetition number $c_{t-1} = 10$. After Δt seconds, the controller is required to make a decision based on state s_t at the beginning of time interval t. Because of action $a_{t-1} = 0$, the controller obtains x_t where $\phi_t = 1, c_t = 11$ and $D_t = [3.86, \ 3.12, \ldots, 0.00]$. Then, based on the evaluation of the state $s_t = [x_{t-9}, x_{t-8}, \ldots, x_t]$, the controller selects an action $a_t = 0$, receives feedback j_t and begins the next iteration of time interval $t+1$. Subsequently, the controller selects to change the phase ($a_{t+1} = 1$) at the beginning of time interval $t+1$ based on s_{t+1} where $\phi_{t+1} = \phi_t = 1$ and $c_{t+1} = c_t + 1 = 12$ because of the extending phase decision of time interval t ($a_t = 0$). After $\Delta t_{\text{yellow}} + \Delta t$ seconds, state s_{t+2} for time interval $t+2$ is obtained where ϕ_{t+2} and c_{t+2} take values of 2 and 0 as a result of the phase change decision ($a_{t+1} = 1$). Notice that the yellow phase Δt_{yellow} cannot be ignored considering safety issues for phase changes decisions ($a_t = 1$).

IV. REINFORCEMENT LEARNING FOR TRAFFIC SIGNAL CONTROL

The decision-making stage is achieved through a trained neural network which can determine the best action a_t for state s_t. Two neural networks are constructed to achieve the decision-making: a critic network $\hat{V}(s_t; w)$ to predict the expected cumulative cost and an actor network $\hat{\pi}(a_t|s_t; \theta)$ to calculate the optimal action directly (Section IV-A). In terms of the network structure, we adopt the LSTM network to build the critic network and actor network (Section IV-B) to capture the temporal dynamics. Then, as the parameters are stochastically given initially, we adopt an actor-critic framework, one

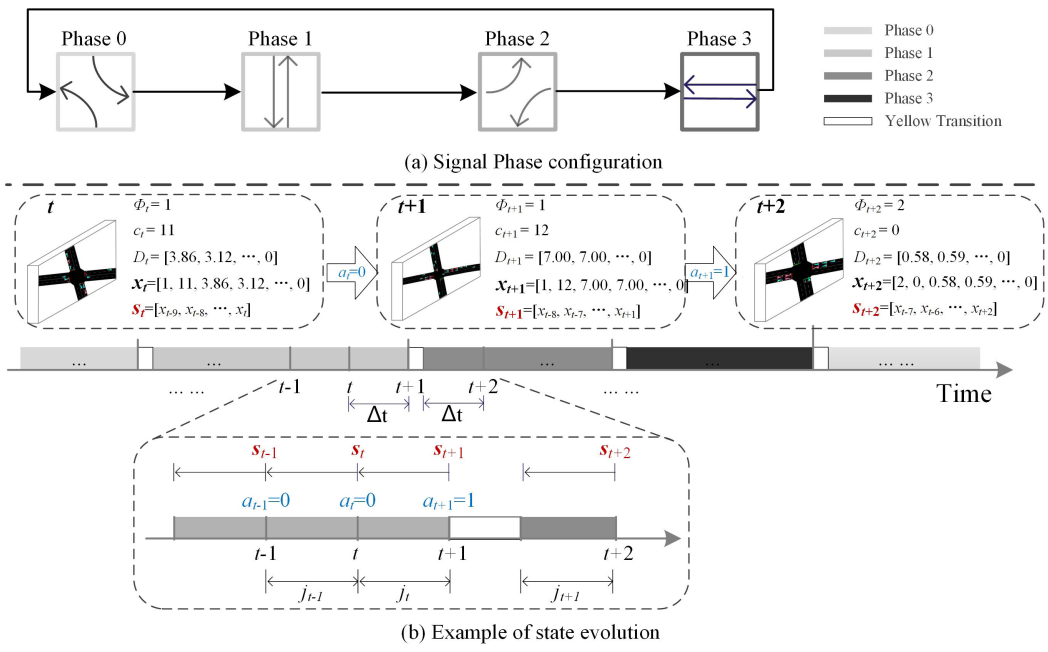
Phase 0
Phase 1
Phase 2
Phase 3
Yellow Transition
(a) Signal Phase configuration
$\Phi_t = 1$
$c_t = 11$
$D_t = [3.86, 3.12, \cdots, 0]$
$x_t = [1, 11, 3.86, 3.12, \cdots, 0]$
$S_t = [x_{t-9}, x_{t-8}, \cdots, x_t]$
$a_t = 0$
$\Phi_{t+1} = 1$
$c_{t+1} = 12$
$D_{t+1} = [7.00, 7.00, \cdots, 0]$
$x_{t+1} = [1, 12, 7.00, 7.00, \cdots, 0]$
$S_{t+1} = [x_{t-8}, x_{t-7}, \cdots, x_{t+1}]$
$a_{t+1} = 1$
$\Phi_{t+2} = 2$
$c_{t+2} = 0$
$D_{t+2} = [0.58, 0.59, \cdots, 0]$
$x_{t+2} = [2, 0, 0.58, 0.59, \cdots, 0]$
$S_{t+2} = [x_{t-7}, x_{t-6}, \cdots, x_{t+2}]$
Time
Δt
$a_{t-1}=0$
j_{t-1}
j_t
j_{t+1}
(b) Example of state evolution

FIGURE 3. Example of state evolution.

type of the RL-based algorithms, to calculate the parameters w and θ in order to reduce the estimated error for the critic network and reduce the future cost for the actor network (Section IV-C). The main logic is to obtain a set of optimal parameters w and θ gradually to guide the process of decision making through training data, which is determined through multiple interactions between the decision-making agent and simulated environment. Furthermore, we adopt two techniques to enhance the algorithm efficiency and robustness, which are Multistep bootstrapping (Section IV-D) and Clipped surrogate objective technique (Section IV-E). Finally, the overall algorithm is given in Section IV-F to illustrate the training details.

A. BASIC COMPONTENTS

RL, a type of machine learning technique, enables the controller to obtain optimal parameters for decision-making agent through trail and error interactions between the controller and simulated environment [18]. Two core concepts in RL are the actor and critic: the actor can guide the choice of action a_t based on state s_t at each time interval t for the controller, and the critic can predict the cumulative cost of state s_t to estimate the long term performance of current state.

The actor can be defined as a conditional probability, $\pi(s, a) = P(a_t = a|s_t = s)$, which can map system state s to an action probability distribution over an action set $a_t \in \{0, 1\}$.

The critic can estimate the average expected cumulative cost since state s_t over the planning horizon $[t, t+1, \ldots, \tau, \ldots, T]$:

$$V(s_t) = \mathbb{E}[\sum_{\tau=t}^{T} j_\tau | s_t] \tag{8}$$

Furthermore, based on the Bellman equation, we can obtain $V(s_t)$ iteratively by using the cost j_t and the next state value $V(s_{t+1})$.

$$V(s_t) = \mathbb{E}[j_t + V(s_{t+1})|s_t] \tag{9}$$

Note that the true values of $V(s_t)$ and $\pi(s, a)$ are difficult to observe in practice. Usually, we adopt function approximations $\hat{V}(s_t; w)$ and $\hat{\pi}(a_t|s_t; \theta)$ to estimate $V(s_t)$ and $\pi(a_t|s_t)$ where w and θ are the parameters of the function approximations $\hat{V}(s_t; w)$ and $\hat{\pi}(a_t|s_t; \theta)$ (shown in Fig. 4).

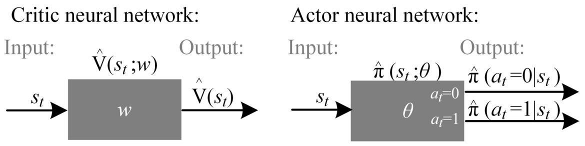

FIGURE 4. Illustrations of critic neural network and actor network.

B. NEURAL NETWORK STRUCTURE USING THE LSTM

To capture the temporal dynamics of the sequences, a long short-term memory (LSTM) network is employed to construct the function approximation.

This study adopts the many to one structure to map a sequence vector $[x_1, x_2, \ldots, x_\tau]$ to vector y_τ [44], as shown in Fig. 5. The LSTM network can be referred as $\Theta^L : \mathbb{R}^{\tau \cdot M} \rightarrow \mathbb{R}^{1 \cdot N}$, where τ is the length of the time sequence, M is the length of one vector and N is the length of the output. In addition, fully connected layer can be referred as $\Theta^C : \mathbb{R}^M \rightarrow \mathbb{R}^N$, where M denotes the length of the input vector and N denotes the length of the output vector.

The function approximation architecture adopted in this study is shown in Fig. 5. For each time interval, t, the state

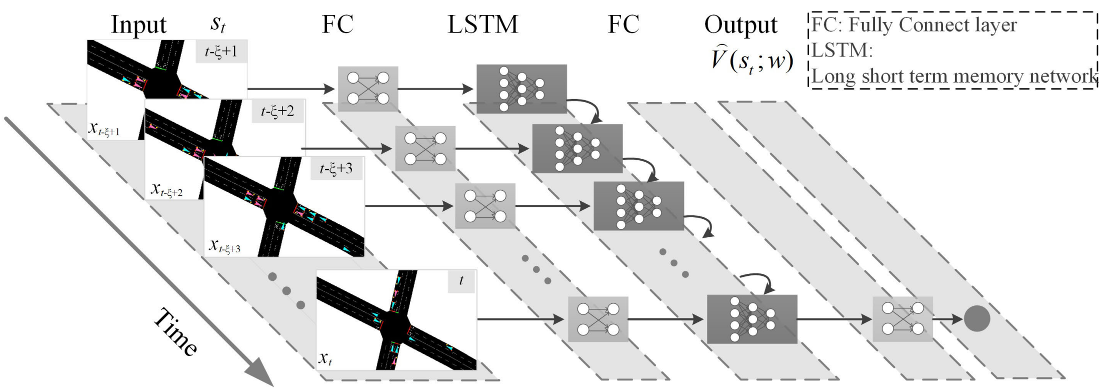

FIGURE 5. **Architecture of the Critic Network using the LSTM Network.**

$s_t = [x_{t-\xi+1}, x_{t-\xi+2}, \ldots, x_t]$ is obtained through stacking a series of spatial observations $x_{t-\xi+1}, x_{t-\xi+2}, \ldots, x_t$ of different time intervals, where ξ is the length of the time series and the length of each x_t is $N_i + 2$ (see Section IV-C). Using state s_t as the input, the input matrix size is $\xi \cdot (N_i + 2)$. First, we employ a fully connected layer Θ^C with 64 neurons and rectifier nonlinear activation functions to compress observation $x_\tau \quad \tau \in [t - \xi + 1,\ t - \xi + 2,\ \ldots, t]$. Then, we pass the stacked output to the LSTM layer, Θ^L, where the LSTM layer is composed of 64 units and unrolled for a ξ step input. Finally, the fully connected layer Θ^C is used as the linear output layer with no activation function for the critic and softmax activation function for the actor, where the number of neurons is 1 and 2 respectively, corresponding to the number of outputs in the critic and actor. During the training process, the algorithm uses the Adam optimizer as the gradient descent algorithm with a learning rate of 0.0002 for the critic and 0.0001 for the actor. The critic and actor net use the same structure except for the output layer. The definitions of the critic and actor net are given as follows:

$$\begin{aligned}
&\hat{V}(s_t; w) \\
&\quad = \Theta^C \Theta^L([\Theta^C(x_{t-\xi+1}), \Theta^C(x_{t-\xi+2}), \ldots, \Theta^C(x_t)]) \\
&\quad = \Theta_w(s_t; w) \qquad (10) \\
&\hat{\pi}(a_t|s_t; \theta) \\
&\quad = \Theta^C \Theta^L([\Theta^C(x_{t-\xi+1}), \Theta^C(x_{t-\xi+2}), \ldots, \Theta^C(x_t)]) \\
&\quad = \Theta_\theta(a_t|s_t; \theta) \qquad (11)
\end{aligned}$$

C. PARAMETER OPTIMIZATION USING ACTOR-CRITIC ALGORITHM

The actor-critic algorithm, one of the RL-based algorithms, is adopted in this study to determine the controller's internal parameters (w and θ) in the interactive process between the traffic signal controller and the simulation environment. The reasons for adopting the actor-critic algorithm are that the convergency results in critic-only algorithms tend to be biased and that the convergency speeds in actor-based algorithms are usually rather slow. On the other hand, the actor-critic algorithm effectively provides an appealing trade-off between optimality and convergency speeds.

Two basic components are the actor $\hat{\pi}(a_t|s_t; \theta)$ and critic $\hat{V}(s_t; w)$. During the training process, the actor is employed to determine an action $\hat{\pi}(a_t|s_t; \theta)$ for the current state s_t; then the controller executes the command a_t, receives the feedback j_t and collects the training sample (s_t, a_t, j_t, s_{t+1}); based on the collected sample, the critic can estimate the long-term performance $\hat{V}(s_t; w)$ and get involved in the parameter optimizing process to help the actor and the critic achieve better performance in the future [45]. The actor-critic algorithm optimizes internal parameters θ and w as follows:

(1) the actor chooses action $a_t \sim \hat{\pi}(a_t|s_t; \theta)$ at the beginning of time interval t;

(2) the controller receives the feedback j_t and s_{t+1} at the end of time interval t;

(3) the controller collects the training sample (s_t, a_t, j_t, s_{t+1});

(4) the critic evaluates the temporal difference (TD) error according to the sample;

(5) the algorithm optimizes the actor and the critic's internal parameters θ and w respectively, according to the TD error.

In the following, we will show the details for the parameter optimization process.

For the critic, the parameter w is optimized to decrease the difference between the approximation $\hat{V}(s_t; w)$ and true value $V(s_t)$ by applying a gradient descent to the mean-square loss function $L(w)$.

$$\min_w \ \mathrm{L}(w) = \mathbb{E}[(j_t + \hat{V}(s_{t+1}; w) - \hat{V}(s_t; w))^2] = \mathbb{E}[\delta_t^2] \qquad (12)$$

where $j_t + \hat{V}(s_{t+1}; w)$ is an approximate estimate for the true value $V(s_t)$ following Bellman Equation. $\delta_t = j_t + \hat{V}(s_{t+1}; w) - \hat{V}(s_t; w)$ is temporal difference error (TD error) to express the difference between approximation and true value. The critic optimizing can be regarded as a regression problem to build the mapping between state s_t and value $V(s_t)$ using the training sample (s_t, a_t, j_t, s_{t+1}), where the input label is s_t and the output label is $j_t + \hat{V}(s_{t+1}; w)$. The batch stochastic gradient descent technique (BGSD) is employed to obtain an optimized parameter w: $w \leftarrow w + \alpha_w \delta_t \nabla_w \hat{V}(s_t; w)$, where α_w is the learning rate of the critic.

For the actor, parameter θ is adjusted to minimize the total cost J by applying gradient ascent to the cross-entropy loss $L(\theta)$:

$$\min_{\theta} \ \mathrm{L}(\theta) = \mathbb{E}[\log \pi(a_t|s_t; \theta)\delta_t] \tag{13}$$

Eq. 13 can optimize θ using the BGSD technique following $\theta \leftarrow \theta + \alpha_\theta \delta_t \nabla_\theta \log \pi(a_t|s_t; \theta)$, where α_θ is the learning rate in the actor. For further theoratical explaination, readers can refer to the work by Sutton [18].

The whole procedure of the actor-critic algorithm is summarized in Algorithm 1.

Algorithm 1 Actor Critic Algorithm

```
Input: a differentiable state value function, $\hat{V}(s_t; w)$
       a differentiable policy function, $\hat{\pi}(a_t|s_t; \theta)$
Output: updated parameters $w$ and $\theta$
1:  for day = $0, 1, 2, \ldots, M$ do
2:      for $t = 0, 1, 2, \ldots, T$ do
3:          // Training sample collecting
4:          Sample action $a_t \sim \hat{\pi}(a_t|s_t; \theta)$
5:          Execute the action $a_t$, receive the feedback $j_t$, and
            obtain the next state, $s_{t+1}$
6:          // Parameter optimizing
7:          Compute TD error $\delta_t$ according to the training sample $(s_t, a_t, j_t, s_{t+1})$
8:          Optimize parameters $w$ and $\theta$ using Eqs. 12 and 13
9:      end for
10: end for
11: return Parameters $w$ and $\theta$
```

D. MULTISTEP BOOTSTRAPPING TECHNIQUE

Since the batch size is too small (only one training sample) for parameter optimizing process, we are inspired by the multi-step bootstrapping technique to increase batch size when optimizing parameters. This can further improve the convergency speed and algorithm stability in the above algorithm (Algorithm 1).

The original method updates parameters w and θ using only one sample (s_t, a_t, j_t, s_{t+1}) at the end of each time interval. Inspired by the multistep bootstrapping technique, this study updates parameters w and θ at the beginning of the time interval $t = qn$ for $q = 0, 1, 2, \ldots, Q$, where n is a prespecified number (step) of time intervals. Consider the environment is at time interval $t = qn$, the algorithm progresses as follows: the controller selects actions $a_t \sim \pi(a|s_t; \theta_{qn})$ during the intervals $t = qn, qn+1, \ldots, qn+n-1$ and executes parameter optimizing until the end of the time interval $t = qn+n-1$. The RL algorithm collects the samples (s_t, a_t, j_t, s_{t+1}) from $t = qn$ to $qn + n - 1$ and saves these samples into training buffer $B_{[qn,(q+1)n]}$:

$$B_{[qn,(q+1)n]} = \begin{bmatrix} (s_{qn}, a_{qn}, j_{qn}, s_{qn+1}) \\ (s_{qn+1}, a_{qn+1}, j_{qn+1}, s_{qn+2}) \\ \cdots \\ (s_{qn+n-1}, a_{qn+n-1}, j_{qn+n-1}, s_{(q+1)n}) \end{bmatrix}.$$

Therefore, we can obtain a batch of n-step-TD errors at $t = q + n - 1$ based on $B_{[qn,(q+1)n]}$ using the n-step return:

$$\delta_i = -\hat{V}(s_i; w) + \sum_{\tau=i}^{qn+n-1} j_\tau + \hat{V}(s_{(q+1)n}; w) \quad i \in [qn, qn+1, \ldots, qn+n-1] \tag{14}$$

Using Eq. 14, we can obtain $\delta_{qn}, \ \delta_{qn+1}, \ldots, \delta_{qn+n-1}$ as:

$$\begin{aligned} \delta_{qn} &= -\hat{V}(s_{qn}; w) + j_{qn} + \ldots + j_{qn+n-1} + \hat{V}(s_{(q+1)n}; w) \\ \delta_{qn+1} &= -\hat{V}(s_{qn+1}; w) + j_{qn+1} + \ldots + j_{qn+n-1} + \hat{V}(s_{(q+1)n}; w) \\ &\cdots \\ \delta_{qn+n-1} &= -\hat{V}(s_{qn+n-1}; w) + j_{qn+n-1} + \hat{V}(s_{(q+1)n}; w) \end{aligned}$$

Then, we obtain the expanded training buffer $\tilde{B}_{[qn,(q+1)n]}$:

$$\tilde{B}_{[qn,(q+1)n]} = \begin{bmatrix} (s_{qn}, a_{qn}, j_{qn}, \delta_{qn}, s_{qn+1}) \\ (s_{qn+1}, a_{qn+1}, j_{qn+1}, \delta_{qn+1}, s_{qn+2}) \\ \cdots \\ (s_{qn+n-1}, a_{qn+n-1}, j_{qn+n-1}, \delta_{qn+n-1}, s_{(q+1)n}) \end{bmatrix}$$

We then draw random samples uniformly from the expanded training buffer $\tilde{B}_{[qn,(q+1)n]}$ and adopt these samples to construct a training batch to optimize the parameters w and θ using the BGSD technique based on Eqs. 12 and 13. Compared to optimizing using only a single training sample (see Algorithm 1), batch optimizing calculates a series of TD errors $[\delta_{qn}, \delta_{qn+1}, \ldots, \delta_{qn+n-1}]$ to calculate parameters w and θ.

The process of the multistep bootstrapping technique is visualized in Fig. 6.

E. CLIPPED SURROGATE OBJECTIVE TECHNIQUE

Despite the Actor-Critic Algorithm serves as an effective framework to obtain optimized parameters in the RL agent, the extreme large loss (Eqs. 12 and 13) may cause the parameters change unstably between two successive parameter optimizing processes. This may have a negative impact on the stability of algorithm and convergency speed [46]. Therefore, to alleviate the influence of this problem, this study further employs a clipped surrogate objective technique to improve algorithm robustness. The clipped surrogate objective technique uses clipped probability ratios to enhance the performance of parameter updating.

After implementation in the clipped surrogate objective technique, the actor loss function $L(\theta)$ is modified as follows:

$$\min_{\theta} L(\theta) = \mathbb{E}\{\min[\delta_t \varepsilon_t(\theta), \ \delta_t \mathrm{clip}(\varepsilon_t(\theta), \ 1-\epsilon, \ 1+\epsilon)]\} \tag{15}$$

where the clip ratio is defined as $\varepsilon_t(\theta) = \frac{\pi(a_t|s_t;\theta)}{\pi(a_t|s_t;\theta_{\text{old}})}$ and ϵ is the clip rate. θ_{old} is the previous value of the policy neural

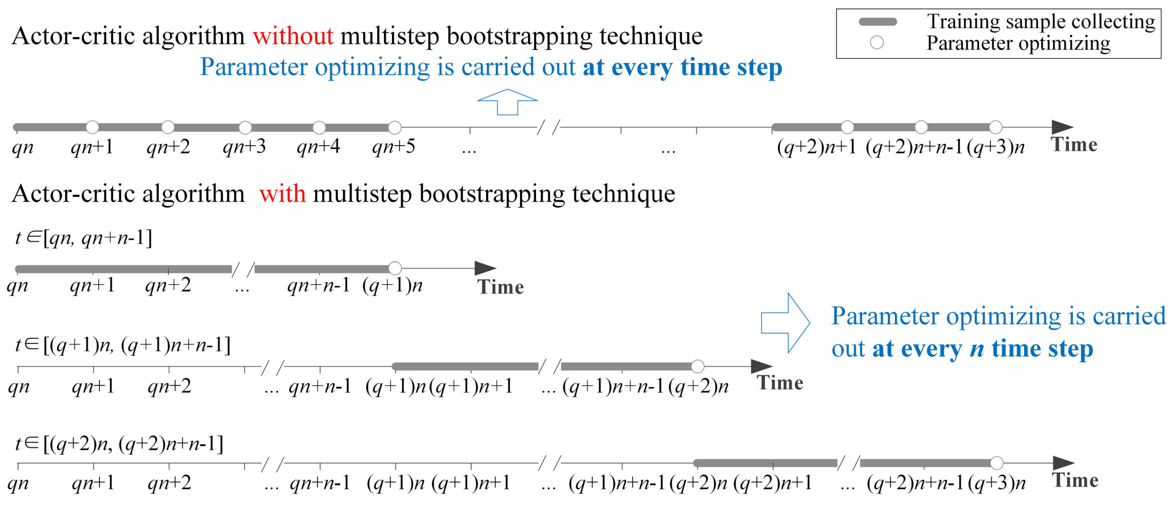
Training sample collecting
Parameter optimizing
Actor-critic algorithm without multistep bootstrapping technique
Parameter optimizing is carried out at every time step
qn qn+1 qn+2 qn+3 qn+4 qn+5 ... ... (q+2)n+1 (q+2)n+n-1 (q+3)n Time
Actor-critic algorithm with multistep bootstrapping technique
t∈[qn, qn+n-1]
qn qn+1 qn+2 ... qn+n-1 (q+1)n Time
Parameter optimizing is carried out at every n time step
t∈[(q+1)n, (q+1)n+n-1]
qn qn+1 qn+2 ... qn+n-1 (q+1)n (q+1)n+1 ... (q+1)n+n-1 (q+2)n Time
t∈[(q+2)n, (q+2)n+n-1]
qn qn+1 qn+2 ... qn+n-1 (q+1)n (q+1)n+1 ... (q+1)n+n-1 (q+2)n (q+2)n+1 ... (q+2)n+n-1 (q+3)n Time

FIGURE 6. Illustration of the multistep bootstrapping technique.

network parameter. This indicates a conservative attitude in parameter optimizing [47]. The clip function is defined as follows:

$$\text{clip}(x, min, max) = \begin{cases} min & \text{if } x < min, \\ x & \text{if } min < x < max, \\ max & \text{if } x > max. \end{cases} \quad (16)$$

Therefore, $\text{clip}(\varepsilon_t(\theta), 1-\epsilon, 1+\epsilon)$ can guarantee that the effective $\varepsilon_t(\theta)$ is in the interval $[1-\epsilon, 1+\epsilon]$, which enables the algorithm to avoid the trap of excessive parameter changes. Finally, the minimum value between $\delta_t\varepsilon_t(\theta)$ and clipped $\delta_t\varepsilon_t(\theta)$ is adopted in calculating the loss function of parameter θ, which can provide a pessimistic bound for the loss function $L(\theta)$ and avoid the problem of oscillation caused by large parameter changes.

F. OVERALL ALGORITHM

In this section, we summarize the above content and provide an overall algorithm for the training of the controller internal parameters w and θ. The overall algorithm, shown in Algorithm 2, is an actor-critic algorithm combined with a multistep bootstrapping technique and a clipped surrogate objective technique.

In Algorithm 2, the time interval t is the minimum traffic signal control unit in the planning period with a duration of Δt. We define the operator $*$ to show the real-time of time interval t in the environment where the relationship of time interval $t+1$ and t is $(t+1)^* = t^* + \Delta t$ if $a_t = 0$ or $(t+1)^* = t^* + \Delta t_{\text{yellow}} + \Delta t$ if $a_t = 1$. The controller consists of two parts: an actor $\hat{\pi}(a_t|s_t;\theta)$ and a critic $\hat{V}(s_t;w)$. Moreover, we adopt a deep neural network to construct the functions $\hat{V}(s_t;w)$ and $\hat{\pi}(a_t|s_t;\theta)$ (see Section IV-B).

The control process is as follows: at the beginning of each time interval t, the controller observes the state s_t selects an action a_t and sends it to the traffic light; after Δt (for $a_t = 0$) or $\Delta t_{\text{yellow}} + \Delta t$ (for $a_t = 1$) seconds, the controller receives the feedback j_t and observes the next state s_{t+1} to begin the next iteration. The duration of the planning period is referred to as Γ, and the simulation of one day terminates when the actual time $T^* \geq \Gamma$. As a common practice in RL, the state value of the terminal state $V(s_T)$ is equal to 0. The action a_t

Algorithm 2 Training Controller Internal Parameters by RL

```
Input:  a differentiable state value function $\hat{V}(s_t;w)$
        a differentiable policy function $\hat{\pi}(a_t|s_t;\theta)$
Output: optimized parameters $w$ and $\theta$
 1: Initialization $\theta = \theta_0$, $w = w_0$, $q = 0$
 2: for day $= 0, 1, 2, \dots, M$ do
 3:     $q = 0$
 4:     for $t = 0, 1, 2, \dots, T$ do
 5:         // Training sample collecting
 6:         Sample action $a_t \sim \hat{\pi}(a_t|s_t;\theta)$
 7:         Execute the action $a_t$, receive the feedback $j_t$ and
            obtain the next state $s_{t+1}$
 8:         Store sample $(s_t, a_t, j_t, s_{t+1})$ to the training buffer
            $B_{[qn,(q+1)n]}$
 9:         // Parameter optimizing
10:         if $t+1 = (q+1)n$ or the simulation of one day ends
            then
11:             Compute a batch of n-step TD errors
                $[\delta_{qn}, \delta_{qn+1}, \dots, \delta_{qn+n-1}]$ and construct the
                expanded training buffer $\tilde{B}_{[qn,(q+1)n]}$ based on
                (14).
12:             Optimize parameters $w$ and $\theta$ using the expanded
                training buffer $\tilde{B}_{[qn,(q+1)n]}$ based on (12) and (15).
13:             $q = q + 1$
14:         end if
15:     end for
16: end for
17: return Parameters $w$ and $\theta$
```

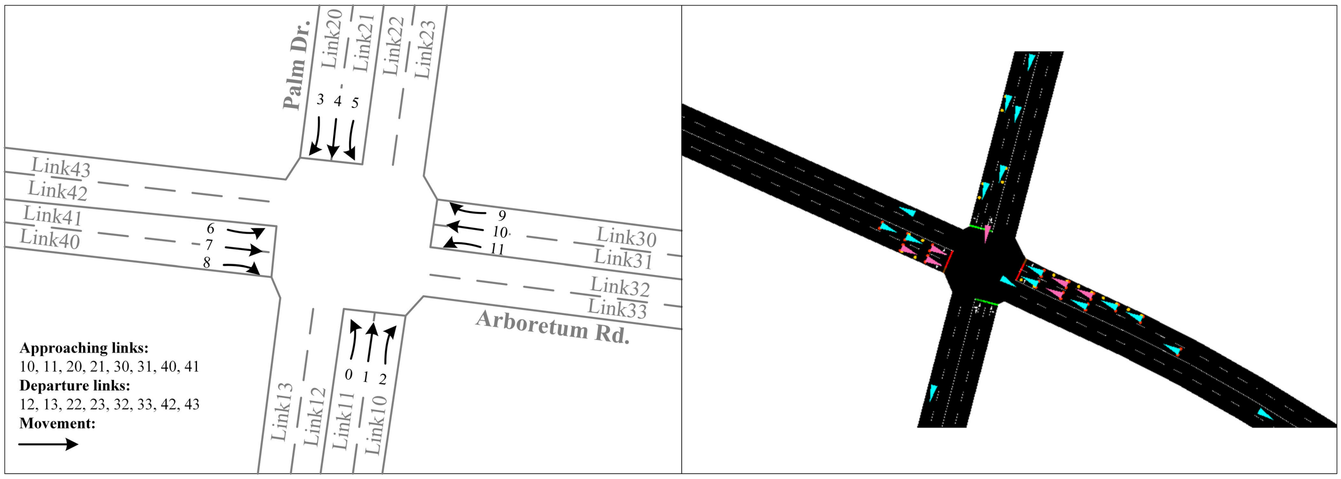

(a) Selected Intersection Layout (b) Simulation Example in SUMO

FIGURE 7. Selected Intersection in the simulation of SUMO.

is a binary variable, where the value 0 denotes remaining in the current phase and the value 1 denotes switching into the next phase.

Using a multistep bootstrapping technique, we can divide the planning period into a training sample collecting period (interaction process between traffic environment and controller) and a parameter optimizing period (the parameter optimizing process to optimize parameters θ and w).

(1) Training sample collecting period (time duration $t = [qn, qn + 1, \ldots, qn + n - 1]$)

For each time interval t, the controller selects an action $a_t \sim \pi(a|s_t; \theta_{qn})$ and sends the command a_t to the traffic light to control the movement of the vehicles; the controller then receives the feedback j_t and begins with s_{t+1} after Δt or $\Delta t_{\text{yellow}} + \Delta t$ seconds. Then, the controller collects the sample (s_t, a_t, j_t, s_{t+1}) and stores it in the training buffer $B_{[qn,(q+1)n]}$. The controller starts at time interval qn and repeats the above interaction process n times until time interval $qn + n - 1$.

(2) Parameter optimizing period (the end of time interval $qn + n - 1$)

If the next time interval $t + 1 = (q + 1)n$ or the controller terminates in the next time interval (when $(t + 1)^* > \Gamma$), the controller computes a batch of advantaged estimators $[\delta_{qn}, \delta_{qn+1}, \ldots, \delta_{qn+n-1}]$ and constructs the expanded the training buffer $\tilde{B}_{[qn,(q+1)n]}$.

Finally, the controller optimizes parameters w and θ using the BGSD technique.

The traffic signal control algorithm is summarized in Algorithm 2.

V. EXPERIMENTS AND RESULTS

In this section, we provide a series of numerical examples to demonstrate the performance of the proposed traffic signal control method. The microscopic traffic simulator SUMO (Simulation of Urban Mobility) was used as the simulation environment in our experiments [48]. The vehicle agent communicates with the traffic environment through the TraCI package of SUMO. We implemented the LSTM networks using TensorFlow 1.5 to approximate the functions $\hat{V}(s_t; w)$ and $\hat{\pi}(a_t|s_t; \theta)$ [49]. The tests were executed on a desktop PC with a 4.20 GHz i7-7700 CPU, 32 GB of RAM running Windows 10. The whole procedure was implemented in Python 3.5.

A. STUDY AREA

This numerical example is based on the test bed introduced by Jeffrey Glick [50]. The selected intersection is located at the intersection of Palm Drive and Arboretum Road, in Stanford CA 94305, USA. The corresponding SUMO configurations were exported from OpenStreetMap.org, as shown in Fig. 7. The given intersection has four direction legs, and each approaching and departure leg comprises two links. In each approaching link, the movement m can choose to move left, through or right in accordance with their route U.

B. TRAFFIC DEMAND AND VEHICLE GENERATION

In this section, we introduce a vehicle arrival generation method based on the realistic traffic demands (hourly traffic volume data of different vehicular movements). In practice, it is common to collect the hourly traffic volume data (vehicles per hour, vph) for 12 movements (4 left-turn movements, 4 through movements and 4 right-turn movements), as shown in Fig. 7. The 24-hour traffic volume data for the 12 movements is used for the test, as shown by the gray points in Fig. 8. These traffic flow data were sourced from the Github project by Jeffrey Glick [50]. To describe the traffic flow time-dependent characteristics, we adopt 12 polynomial fitted functions $[\rho_0(t), \rho_1(t), \ldots, \rho_m(t), \ldots, \rho_{11}(t)]$ to approximate the time-dependent traffic demand of the

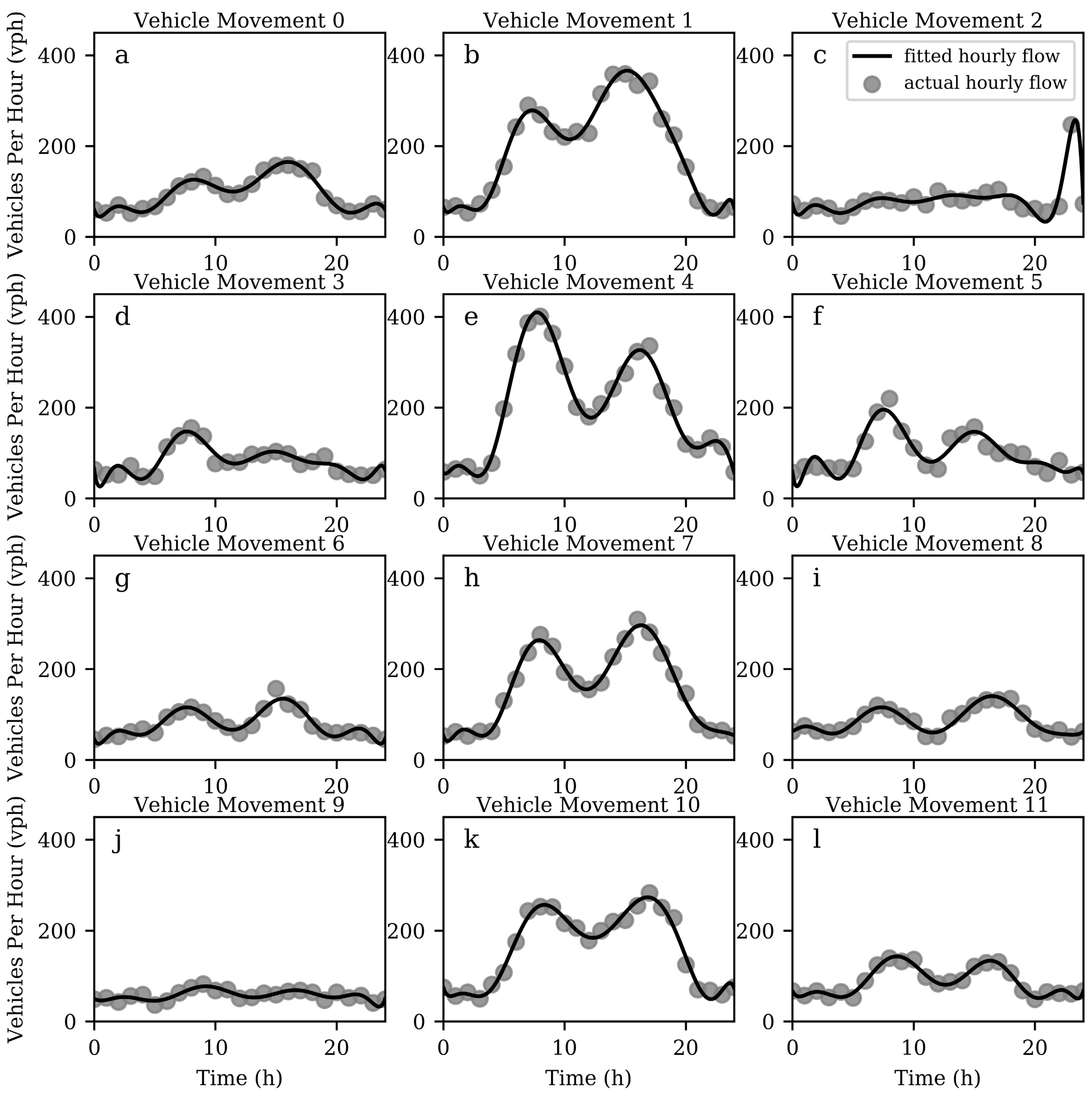

FIGURE 8. Traffic flow of the 12 movements.

12 traffic movements. The black curve in Fig. 8 represents the time-related characteristics of the traffic demand $\rho_m(t)$. Therefore, we can insert the vehicles into the network dynamically and stochastically to reflect the morning and evening peaks, which creates a realistic and varying flow pattern for the agent to control, as opposed to using a constant hourly demand.

To simulate a series of stochastic traffic scenarios in SUMO, we assume that the vehicles arrive upstream of the approach to the intersection following a Poisson distribution with a time-dependent arrival rate of $\lambda = \rho_m(t)$. For vehicles $k \in U^m$, they follow the direction of movement m, where U^m denotes all the vehicles in movement m. Therefore, for vehicles $k \in U^m$ in movement m, the headway $\Delta\zeta$, of two adjacent vehicles $k+1$ and k follows the negative exponential distribution:

$$\Delta\zeta \sim \lambda e^{-\lambda\Delta\zeta} \quad \text{where } \lambda = \rho_m(\zeta(k)) \tag{17}$$

where $\Delta\zeta$ indicates the headway between two adjacent vehicles $k+1$ and k. $\zeta(k)$ indicates the departing time of vehicle k. The arrival rate λ is estimated using the fitted function $\rho_m(t)$ (see the black curve in Fig. 8).

C. PARAMETER SETTINGS

To train the parameters in the LSTM network using RL, we run the numerical experiment for an arbitrary figure of 200 simulated days, using the standard 86400 seconds for the duration of each day. The exploration rate drops from 1.0 to 0.0 linearly during the first 150 days. After the 150th day, the agent stops exploring and exploits the

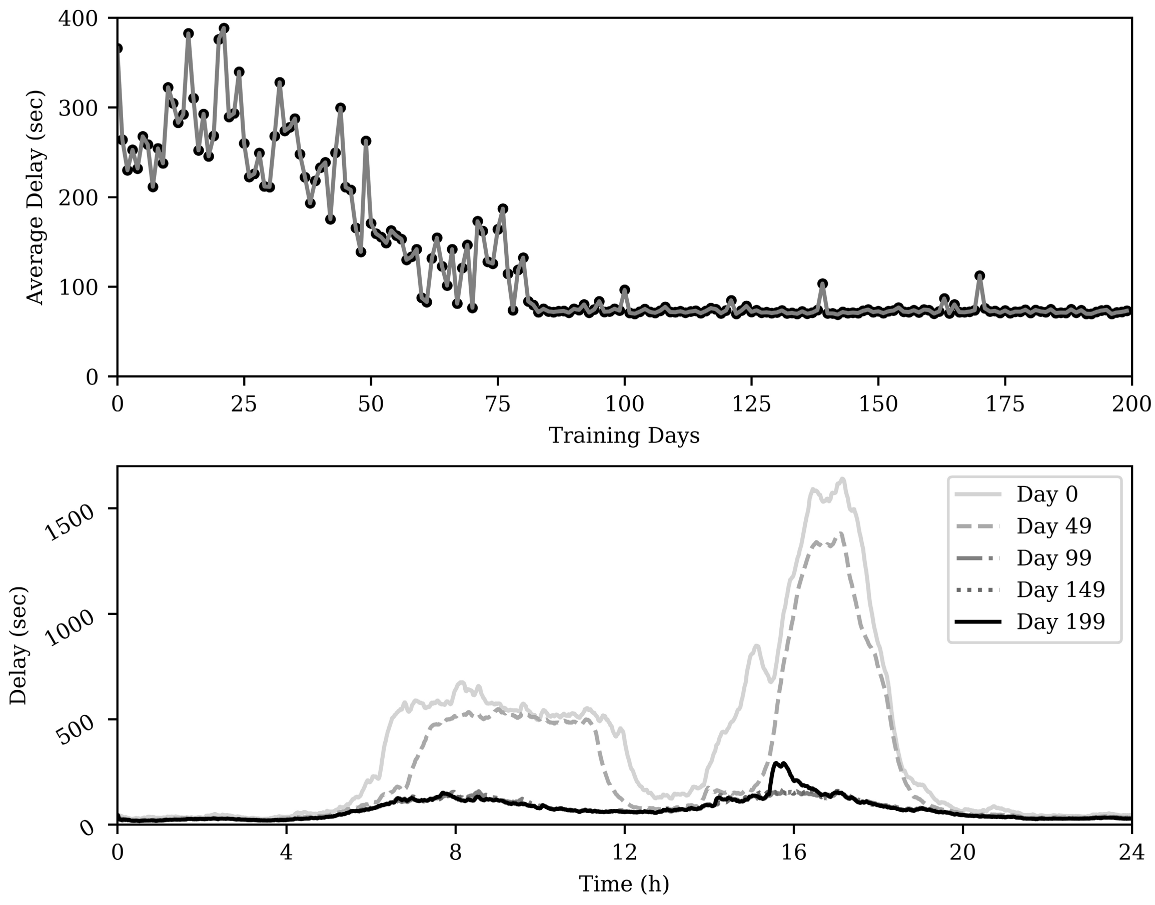

FIGURE 9. Learning process over 200 days.

TABLE 1. Hyper-parameters setting.

Hyper-parameters	Meaning	Values
Γ	duration of the whole planning period	$24 \cdot 60 \cdot 60$ seconds
Δt	duration of each time step	7 seconds
Δt_{yellow}	duration of yellow transition	4 seconds
n	length of sampling period	32
ξ	the length of time sequences in LSTM	40
ϵ	clip rate	0.2

TABLE 2. Synchro signal time settings.

Hour	Cycle	PH0	YT	PH1	YT	PH2	YT	PH3	YT
0 h -5 h	60	6	4	16	4	6	4	16	4
5 h -7 h	60	6	4	16	4	5	4	17	4
7 h -10 h	60	6	4	17	4	4	4	17	4
10 h -15 h	60	5	4	18	4	4	4	17	4
15 h -18 h	60	6	4	17	4	4	4	17	4
18 h -20 h	60	6	4	18	4	4	4	16	4
20 h -24 h	60	6	4	16	4	6	4	16	4

[a] PH: Phase Duration (seconds); YT: Yellow Transition Duration (seconds).

environment completely. The learning rates are 0.0002 and 0.0001 for critics and actors, respectively. The hyper-parameter settings are shown in Table 1.

D. BENCHMARK GENERATED BY SYNCHRO

We evaluate the effectiveness of the algorithm relative to the fixed-time controller generated by Synchro [31]. Synchro has been widely recognized as a practical software tool for developing a fixed time schedule for traffic signal control. Based on historical demand, the software calculated the best cycle length to be 60 seconds. To reflect fluctuations in the traffic demand, we divide the 24 hours demand into 7 subsets, and each configuration is shown in Table 2. Additionally, the yellow transition is set to 4 seconds between two different phases, which is included at the end of each phase.

E. RESULTS ANALYSIS

1) CONVERGENCE VALIDATION

The performance of the agent during the training process is shown in Fig. 9. The horizontal axis of the figure reflects the training days, ranging from 0 to 200, where a day represents a simulated day. The vertical axis reflects the average cost $\frac{J}{T}$ (overall delay at the intersection during each time interval). The gray curve illustrates that the value of the objective function can increase significantly during the learning process. The magnitudes of the oscillations decreases

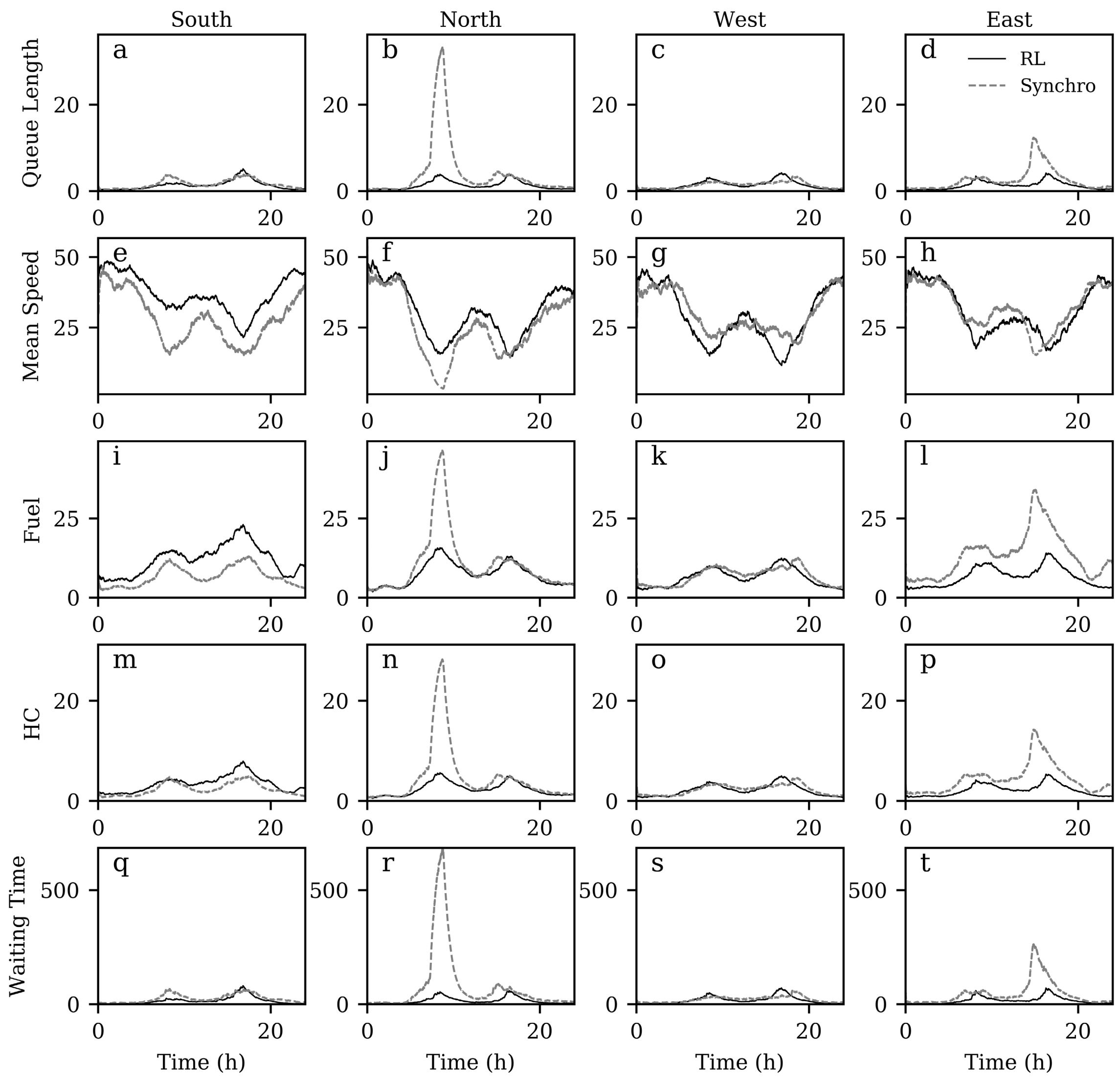

FIGURE 10. Evolutions of the RL controller and fixed-time plan over 24 h: a lower value means better control.

with growing training days. The results confirm that our algorithm can learn from experience and optimize the policy gradually.

To describe the above results in detail, in Fig. 9 (b), the cost j_t during one day, for different days is visualized to provide insight into the noise and performance changes as the algorithm progresses. The horizontal axis represents the simulation time for one day, while the vertical axis is the cost j_t obtained per time interval. Note that we use the moving average technique to illustrate the change tendency of costs during a day. Fig. 9 (b) shows that the cost increases significantly during the morning and evening peaks of all the training days because of commuting traffic, which is consistent with the tendency of the traffic demand in Fig. 8. However, the magnitude of increased delay during the period of commuting, decreases as the training days progress as illustrated through the comparisons between day 0, 49, 99, 149 and 199. Therefore, we can conclude that the influence of the commuting traffic is significantly weakened using our algorithm.

Moreover, Fig. 9 (b) shows the convergence of the proposed RL algorithm. Initially, on training day 0 (day 0), the agent explores the environment and selects actions randomly most of the time. Therefore, the performance of the agent is poor, and the magnitude of the oscillations is very large. As the training days progress, the agent learns more from experience and selects more exploitative actions with a lower exploratory rate. Thus, the agent achieves a lower cost, lower variance and a near-optimal and stable performance to control the environment. Finally, after training day 83, the agent begins to converge to an optimal policy as indicated in Fig. 9 (a).

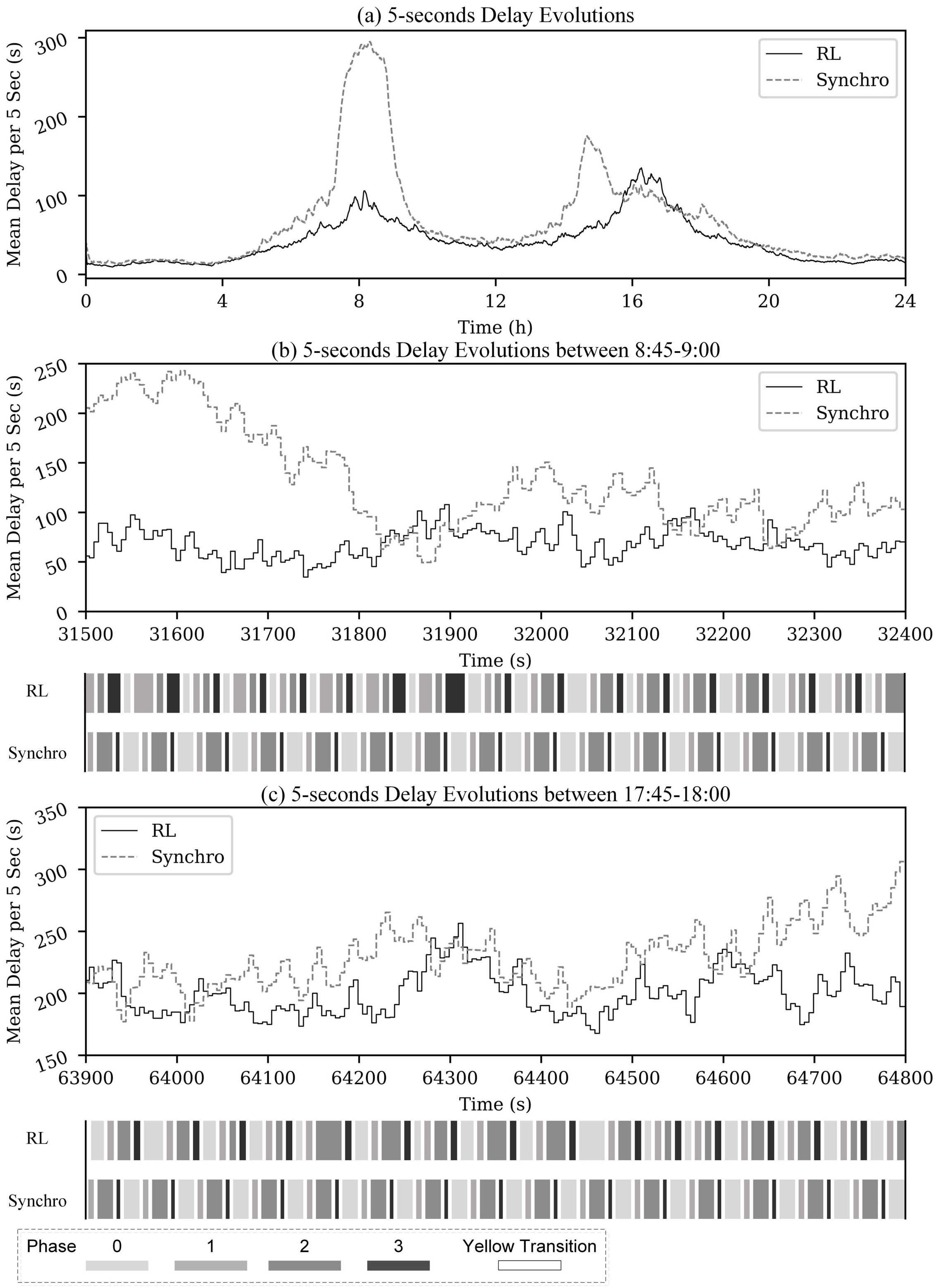

FIGURE 11. Delay evolutions of the RL controller and fixed-time plan over 24 h.

2) PERFORMANCE COMPARISON

We compare the RL controller's performance to that of the fixed-time plan generated by Synchro. As the RL controller has a different cycle length with a fixed-time plan, we collect data every 5 seconds in the RL controller and use a fixed-time plan to build the same test bench. To test the effectiveness

TABLE 3. Performance comparisons of RL controller and fixed time plan (Synchro).

Day	FU		HC		MS		QL		WT	
	SY	RL	SY	RL	SY	RL	SY	RL	SY	RL
0	9.39	8.10	3.43	2.52	28.89	31.71	2.46	1.32	42.90	16.46
1	8.86	8.59	3.02	2.81	28.89	30.49	1.93	1.68	31.47	21.20
2	9.33	8.28	3.38	2.63	28.47	31.12	2.39	1.46	43.03	18.20
3	8.92	8.12	3.11	2.55	29.10	31.36	2.07	1.36	34.92	16.55
4	9.93	8.07	3.80	2.54	28.68	31.42	2.92	1.37	52.78	16.47
5	8.92	8.73	3.07	2.89	28.79	30.78	1.99	1.75	32.95	23.49
6	8.90	8.36	3.06	2.68	28.71	30.94	1.98	1.51	32.77	19.20
7	9.09	8.44	3.18	2.68	28.83	31.39	2.11	1.47	35.83	19.45
8	9.12	8.35	3.19	2.64	28.62	31.24	2.12	1.42	36.03	18.73
9	9.02	8.35	3.13	2.63	28.77	31.22	2.05	1.40	34.71	17.91
Mean	9.15	8.34	3.24	2.66	28.78	31.17	2.20	1.47	37.74	18.77
Impro(%)	8.85		17.92		8.31		33.09		50.27	

[b] FU: Fuel (ml/s); HC: hydrocarbon emission rate (mg/s); MS: mean speed (m/s); QL: queue length (veh); WT: waiting time (s);
SY: synchro plan; RL: reinforcement learning plan; Impro: Improvement.

TABLE 4. Performance comparisons of the RL controller and fixed-time plan (Synchro) for the different directions.

	FU		HC		MS		QL		WT	
	SY	RL	SY	RL	SY	RL	SY	RL	SY	RL
South	6.69	12.01	2.36	3.44	28.04	36.98	1.63	1.32	25.16	15.80
North	10.61	7.44	4.66	2.37	25.22	30.04	4.25	1.31	79.68	15.16
West	6.69	6.31	2.24	2.13	30.18	28.73	1.37	1.37	20.81	18.13
East	13.58	6.62	4.47	2.16	32.12	31.10	2.60	1.26	45.95	16.78
Mean	9.39	8.10	3.43	2.52	28.89	31.71	2.46	1.32	42.90	16.46

[c] FU: Fuel (ml/s); HC: hydrocarbon emission rate (mg/s); MS: mean speed (m/s); QL: queue length (veh); WT: waiting time (s).
SY: synchro plan; RL: reinforcement learning plan.

of the RL controller, we chose an additional 5 indicators, including fuel consumption (ml/s), emissions rate (mg/s), mean speed (m/s), queue length (veh), and waiting time (seconds). Note that waiting time is different from the delay, in that waiting time refers to the stopping time as a result of a red phase, while delay time refers to the extra time needed because of the control policies. With respect to the emissions rate, we only consider hydrocarbon (HC) emissions. In the experiment, we chose 10 random samples to compare the two above control methods (see Table 3). Moreover, we establish performance comparisons by analyzing day 0 (1st sample) in detail. In Table 4 and Fig. 10, we analyze the performance of the four directions in the Synchro and RL controllers. In Fig. 11, we analyze the delay evolution over 24 h, morning peak between 8:45 to 9:00 and evening peak from 17:45 to 18:00.

As listed in Table 3, for 10 random samples, the RL controller can effectively reduce fuel consumptions by 8.85%, emission rates by 17.92%, vehicle queue lengths by 33.09%, waiting times by 50.27% and increase mean speeds by 8.31%. Therefore, we can conclude that the RL controller performs better than the fixed-time plan because it can adapt to real-time changes in traffic flows at a higher resolution.

Table 4 and Fig. 10 show that compared with the fixed-time plan in Synchro, the RL controller can significantly improve the performance of traffic signal control in terms of the five indicators. Fig. 10 shows that the RL controller can enhance the performance of the north direction in the morning peak and the performance of the east direction in the evening. Compared to the fixed-time plan, RL can reduce the queue length from 4.25 to 1.31 and from 2.60 to 1.26 in the north and east directions, respectively (see Table 4). The above result is consistent with the fact that the north traffic (flows 3,4 and 5) and east traffic (flows 9,10 and 11) occupy a large proportion of the traffic in the morning and evening peaks (see Fig. 8). The result shows that the RL controller can address the unbalanced time-space problem caused by commuting traffic.

The delay evolution is illustrated in Fig. 11 (a), and the results show that the RL controller performs better in comparison to the Synchro plan because of the rapid and flexible changing phases. As Fig. 11 (a) shows, the delay in both controllers increases with increasing traffic demand in the morning and evening peaks, whereas the RL controller increases more slowly when compared to the fixed-time controller, especially in the morning peak. Fig. 11 (b) shows that the RL controller can increase the duration of phase 1 (time duration from 31600 to 31900) and phase 3 (time duration from 32000 to 32400) to accommodate the traffic demand in the morning peak. However, the Synchro plan is based on the fixed time plan, which can cause an oversaturated traffic flow at the intersection, and delays using the Synchro plan can increase significantly (i.e., the time duration from 31600 to 31900). Additionally, Fig. 11 (c) shows that the RL controller outperforms the Synchro plan by giving more priority to left-turn traffic (phase 0 and phase 2) in the evening peak. We can conclude that the RL controller can outperform the fixed-time plan because of its adaptability and rapid responsiveness.

VI. CONCLUSION

In this paper, we propose a new adaptive traffic signal control scheme to produce optimized traffic control policies in order to minimize the delay of vehicles passing through intersections. The scheme employs an enhanced algorithm which uses spatial-temporal network information to define the traffic state, where individual vehicle delay is used as a basic measure rather than the aggregate measures of flow rate, flow speed and vehicle queue length as used in previous studies. The proposed method to identify traffic patterns can reduce information loss (such as vehicle delay) when characterizing high-dimensional features in the definition of traffic state. Furthermore, we adopted a deep neural network (the LSTM) to construct a decision-making agent in which its intrinsic parameters are determined through a RL framework; thus optimizing the ability of a traffic controller to decide whether to extend the current phase or switch into the next phase. Specifically, the RL framework uses an actor-critic algorithm to obtain a balance between a biased convergence result (critic-based RL algorithms) and a high variance result (actor-based RL algorithms). Additionally, we modified this algorithm with a multistep technique and a clipped surrogate objective technique to improve its performance.

In the simulations, we built experiments based on a representation of the intersection of Palm Drive and Arboretum

TABLE 5. Variables and meanings.

variable	meaning
Network Configuration	
i	cell index
Ω	set of approaching links
N_i	total number of cells at the approaching links
m	movement index illustrated in Fig. 1
$\rho_m(t)$	approximated time-dependent traffic demand function of movement m
Control Policy	
t	discrete time index
T	total number of time intervals in the planning horizon
Γ	duration of the whole planning period and the planning horizon consists of a sequence of time intervals $0, 1, 2, .., T$
t^*	real time corresponding to time t (seconds)
Δt	duration of a time interval t (seconds)
Δt_{yellow}	duration of a yellow transition (sec)
Vehicle Information	
k	index of a vehicle entering the intersection
$v_t(k)$	average speed of vehicle k during the time interval t (m/s)
v_{free}	free flow speed (m/s)
$d_t(k)$	delay time of vehicle k at time t (seconds)
$\zeta(k)$	arriving time of vehicle k (seconds)
$U_t^{(i)}$	set of vehicles of cell i at time t
U_t	set of vehicles in the whole network at time t
U^m	set of vehicles of movement m
U	set of vehicles of all movements in the whole network
Signal Optimization	
a_t	control variable denoting the action of switching or not, $a_t \in \{0, 1\}$
ϕ_t	phase index, $\phi_t \in \{0, 1, 2, 3\}$
c_t	cumulative repetition number of the current phase until the end of the last time interval
$D_t^{(i)}$	delay observation of cell i at time t (seconds)
D_t	delay of the whole network at time t
x_t	spatial observation at time at time t
s_t	state at time t
j_t	cost obtained at time t (seconds)
Reinforcement learning	
π	stochastic policy $\pi(s, a) = P(a_t = a \mid s_t = s)$
$\hat{\pi}(a_t \mid s_t; \theta)$	actor network function with parameters θ
$B_{[qn,(q+1)n]}$	training buffer to store the samples from time qn to $(q + 1)n - 1$
$V(s_t)$	true state value, $V(s_t) = \mathbb{E}[\sum_{\tau=t}^{T} j_\tau \mid s_t]$
$\hat{V}(s_t; w)$	critic network function with parameter w
δ_t	temporal difference error (TD error)
n	length of the sampling period
ε	clip ratio in the clipped surrogate objective technique
ϵ	clip rate in the clipped surrogate objective technique
Θ^C	fully connected layer
Θ^L	LSTM layer
ξ	the length of the time sequences in the LSTM

Road, where simulated vehicles entered the network based on the assumption that the vehicle arrival rate follows a Poisson distribution that was derived from the 24-hour traffic flow history for this intersection. Therefore, this vehicle generation plan reflects the prevailing time-varying daily commuting traffic, which characterizes the flow peak in rush hours and the instability of traffic flow during non-rush hour periods. Regarding the primary aim of this study, to reduce vehicle delay times at intersections, it was shown in the numerical examples for 10 random samples, compared to the optimized fixed-time plans obtained using Synchro, that the proposed method can reduce such vehicle delay times by over 50%. This significant reduction in delay times also has additional knock-on effects; fuel consumptions were reduced by over 8%, emission rates down by over 17%, vehicle queues down by over 33%, whilst mean speeds were increased by over 8%. The results, therefore, strongly indicate that the proposed scheme should be effective for traffic signal control at isolated intersections where significant traffic fluctuations are prevalent.

The proposed scheme in this study essentially focused on an isolated intersection. However, in future work the scheme could be extended to control a regional network similar to that of the OPAC and PRODYN systems. To overcome the significant computational load problems, a distributive RL framework should also be considered to speed up the training process.

NOTATION

In this section, the notation is given in Table 5 to clarify the whole scheme.

RELATIONSHIP BETWEEN δW, $\delta\theta$ AND $L(W)$, $L(\theta$

$$\begin{aligned}\Delta\theta &= \alpha_\theta \delta_t \nabla_\theta \log \pi(a_t \mid s_t; \theta) \\ &= \mathbb{E}[\log \nabla_\theta \pi(s, a)\delta_t] \\ &= \nabla_\theta L(\theta) \end{aligned} \tag{18}$$

Eq. 18 shows that $\Delta\theta$ is the derivative of $L(\theta)$, where the update gradient $\alpha_\theta \delta_t \nabla_\theta \log \pi(a_t \mid s_t; \theta)$ is the common updating rule of the policy-based RL algorithm. In the study, the automatic differentiate software achieves $\max_\theta L(\theta)$ by obtaining the derivative $\Delta\theta$ to update θ. In other words, the automatic differentiation software (such as TensorFlow, Keras, PyTorch) achieves $\min_w L(w)$ by obtaining the derivative Δw.

REFERENCES

[1] P. Diakaki, D. Kotsialos, and Y. Wang, "Review of road traffic control strategies," *Proc. IEEE*, vol. 91, no. 12, pp. 2041–2042, Dec. 2003.

[2] A. L. C. Bazzan, D. de Oliveira, and B. C. da Silva, "Learning in groups of traffic signals," *Eng. Appl. Artif. Intell.*, vol. 23, no. 4, pp. 560–568, Jun. 2010, doi: 10.1016/j.engappai.2009.11.009.

[3] S. Araghi, A. Khosravi, and D. Creighton, "A review on computational intelligence methods for controlling traffic signal timing," *Expert Syst. Appl.*, vol. 42, no. 3, pp. 1538–1550, Feb. 2015.

[4] D. Zhao, Y. Dai, and Z. Zhang, "Computational intelligence in urban traffic signal control: A survey," *IEEE Trans. Syst., Man, Cybern. C, Appl. Rev.*, vol. 42, no. 4, pp. 485–494, Jul. 2012.

[5] K.-L.-A. Yau, J. Qadir, H. L. Khoo, M. H. Ling, and P. Komisarczuk, "A survey on reinforcement learning models and algorithms for traffic signal control," *ACM Comput. Surv.*, vol. 50, no. 3, pp. 1–38, Jun. 2017. [Online]. Available: http://dl.acm.org/citation.cfm?doid=3101309.3068287

[6] P. Mannion, J. Duggan, and E. Howley, "An experimental review of reinforcement learning algorithms for adaptive traffic signal control," in *Autonomic Road Transport Support Systems*. Springer, 2016, pp. 47–66.

[7] M. Aslani, M. S. Mesgari, and M. Wiering, "Adaptive traffic signal control with actor-critic methods in a real-world traffic network with different traffic disruption events," *Transp. Res. C, Emerg. Technol.*, vol. 85, pp. 732–752, Dec. 2017.

[8] K. Aboudolas, M. Papageorgiou, A. Kouvelas, and E. Kosmatopoulos, "A rolling-horizon quadratic-programming approach to the signal control problem in large-scale congested urban road networks," *Transp. Res. C, Emerg. Technol.*, vol. 18, no. 5, pp. 680–694, Oct. 2010. [Online]. Available: http://www.sciencedirect.com/science/article/pii/S0968090X09000813

[9] H. K. Lo, E. Chang, and Y. C. Chan, "Dynamic network traffic control," *Transp. Res. A, Policy Pract.*, vol. 35, no. 8, pp. 721–744, Sep. 2001. [Online]. Available: http://www.sciencedirect.com/science/article/pii/S0965856400000148

[10] H. K. Lo, "A cell-based traffic control formulation: Strategies and benefits of dynamic timing plans," *Transp. Sci.*, vol. 35, no. 2, pp. 148–164, May 2001. [Online]. Available: http://transci.journal.informs.org/content/35/2/148.abstract

[11] H. K. Lo, "A novel traffic signal control formulation," *Transp. Res. A, Policy Pract.*, vol. 33, no. 6, pp. 433–448, Aug. 1999. [Online]. Available: http://www.sciencedirect.com/science/article/pii/S0965856498000494

[12] P. B. Hunt, D. I. Robertson, R. D. Bretherton, and R. I. Winton, "SCOOT-a traffic responsive method of coordinating signals," Transp. Road Res. Lab., Crowthorne, U.K., Tech. Rep. TRRL LR 1014, 1981.

[13] A. G. Sims and K. W. Dobinson, "The sydney coordinated adaptive traffic (SCAT) system philosophy and benefits," *IEEE Trans. Veh. Technol.*, vol. 29, no. 2, pp. 130–137, May 1980.

[14] S. Sen and K. L. Head, "Controlled optimization of phases at an intersection," *Transp. Sci.*, vol. 31, no. 1, pp. 5–17, Feb. 1997.

[15] Y. Feng, K. L. Head, S. Khoshmagham, and M. Zamanipour, "A real-time adaptive signal control in a connected vehicle environment," *Transp. Res. C, Emerg. Technol.*, vol. 55, pp. 460–473, Jun. 2015. [Online]. Available: http://www.sciencedirect.com/science/article/pii/S0968090X15000091

[16] D. Houli, L. Zhiheng, and Z. Yi, "Multiobjective reinforcement learning for traffic signal control using vehicular ad hoc network," *EURASIP J. Adv. Signal Process.*, vol. 2010, no. 1, Sep. 2010, Art. no. 724035.

[17] L. P. Kaelbling, M. L. Littman, and A. W. Moore, "Reinforcement learning: A survey," *J. Artif. Intell. Res.*, vol. 4, no. 1, pp. 237–285, Jan. 1996.

[18] R. S. Sutton, D. Precup, and S. Singh, "Between MDPs and semi-MDPs: A framework for temporal abstraction in reinforcement learning," *Artif. Intell.*, vol. 112, nos. 1–2, pp. 181–211, Aug. 1999.

[19] J. H. Lee, J. Shin, and M. J. Realff, "Machine learning: Overview of the recent progresses and implications for the process systems engineering field," *Comput. Chem. Eng.*, vol. 114, pp. 111–121, Jun. 2018. [Online]. Available: http://www.sciencedirect.com/science/article/pii/S0098135417303538

[20] D. Silver, A. Huang, C. J. Maddison, A. Guez, L. Sifre, G. van den Driessche, J. Schrittwieser, I. Antonoglou, V. Panneershelvam, M. Lanctot, S. Dieleman, D. Grewe, J. Nham, N. Kalchbrenner, I. Sutskever, T. Lillicrap, M. Leach, K. Kavukcuoglu, T. Graepel, and D. Hassabis, "Mastering the game of go with deep neural networks and tree search," *Nature*, vol. 529, no. 7587, pp. 484–489, Jan. 2016. [Online]. Available: http://www.nature.com/doifinder/10.1038/nature16961

[21] J. Kober, J. A. Bagnell, and J. Peters, "Reinforcement learning in robotics: A survey," *Int. J. Robot. Res.*, vol. 32, no. 11, pp. 1238–1274, 2015. [Online]. Available: http://ijr.sagepub.com/content/32/11/1238

[22] W. Ni and M. J. Cassidy, "Cordon control with spatially-varying metering rates: A reinforcement learning approach," *Transp. Res. C, Emerg. Technol.*, vol. 98, pp. 358–369, Jan. 2019. [Online]. Available: https://www.sciencedirect.com/science/article/pii/S0968090X18312592

[23] J. Barthélemy and T. Carletti, "A dynamic behavioural traffic assignment model with strategic agents," *Transp. Res. C, Emerg. Technol.*, vol. 85, pp. 23–46, Dec. 2017. [Online]. Available: https://www.sciencedirect.com/science/article/pii/S0968090X17302450

[24] S. Richter, D. Aberdeen, and Y. Jin, "Natural actor-critic for road traffic optimisation," in *Proc. Adv. Neural Inf. Process. Syst.*, vol. 19, 2007, p. 1169.

[25] Y. Wang, D. Zhang, Y. Liu, B. Dai, and L. H. Lee, "Enhancing transportation systems via deep learning: A survey," *Transp. Res. C, Emerg. Technol.*, vol. 99, pp. 144–163, Feb. 2019. [Online]. Available: https://www.sciencedirect.com/science/article/pii/S0968090X18304108

[26] J. Ke, H. Zheng, H. Yang, and X. M. Chen, "Short-term forecasting of passenger demand under on-demand ride services: A spatio-temporal deep learning approach," *Transp. Res. C, Emerg. Technol.*, vol. 85, pp. 591–608, Dec. 2017, doi: 10.1016/j.trc.2017.10.016.

[27] T. Zia and U. Zahid, "Long short-term memory recurrent neural network architectures for urdu acoustic modeling," *Int. J. Speech Technol.*, vol. 22, no. 1, pp. 21–30, Nov. 2018.

[28] B. Bakker, "Reinforcement learning with long short-term memory," in *Proc. Adv. Neural Inf. Process. Syst.*, 2002, pp. 1475–1482.

[29] Y. Yin, "Robust optimal traffic signal timing," *Transp. Res. B, Methodol.*, vol. 42, no. 10, pp. 911–924, Dec. 2008. [Online]. Available: http://www.sciencedirect.com/science/article/pii/S0191261508000350

[30] D. I. Robertson, "'TRANSYT' method for area traffic control," *Traffic Eng. Control*, vol. 10, no. 6, pp. 181–182, 1969.

[31] D. Husch and J. Albeck, *Synchro 6: Traffic Signal Software, User Guide*. Albany, CA, USA: Trafficware Corporation, 2003.

[32] J. D. C. Little, M. D. Kelson, and N. M. Gartner, "MAXBAND: A versatile program for setting signals on arteries and triangular networks," *Transp. Res. Rec.*, no. 795, pp. 40–46, 1981.

[33] K. Kyamakya, W. Mathis, R. Stoop, J. C. Chedjou, and Z. Li, *Recent Advances in Nonlinear Dynamics and Synchronization: With Selected Applications in Electrical Engineering, Neurocomputing, and Transportation*, vol. 109. Springer, 2017.

[34] R. A. Vincent and C. P. Young, "Self-optimising traffic signal control using microprocessors. The TRRL MOVA strategy for isolated intersections," *Traffic Eng. Control*, vol. 27, nos. 7–8, pp. 385–387, 1986.

[35] Y. Wang, D. Wang, S. Jin, N. Xiao, Y. Li, and E. Frazzoli, "Iterative tuning with reactive compensation for urban traffic signal control," *IEEE Trans. Control Syst. Technol.*, vol. 25, no. 6, pp. 2047–2059, Nov. 2017.

[36] S. Timotheou, C. G. Panayiotou, and M. M. Polycarpou, "Towards distributed online cooperative traffic signal control using the cell transmission model," in *Proc. 16th Int. IEEE Conf. Intell. Transp. Syst. (ITSC)*, Oct. 2013, pp. 1737–1742.

[37] J.-L. Gallego, J.-L. Farges, and J.-J. Henry, "Design by Petri nets of an intersection signal controller," *Transp. Res. C, Emerg. Technol.*, vol. 4, no. 4, pp. 231–248, Aug. 1996.

[38] C. Cai, C. K. Wong, and B. G. Heydecker, "Adaptive traffic signal control using approximate dynamic programming," *Transp. Res. C, Emerg. Technol.*, vol. 17, no. 5, pp. 456–474, Oct. 2009, doi: 10.1016/j.trc.2009.04.005.

[39] J. J. Henry, "PRODYN tests and future experiments on ZELT," in *Proc. Vehicle Navigat. Inf. Syst. Conf.*, 1989, pp. 292–295.

[40] N. H. Gartner, F. J. Pooran, and C. M. Andrews, "Optimized policies for adaptive control strategy in real-time traffic adaptive control systems: Implementation and field testing," *Transp. Res. Rec., J. Transp. Res. Board*, vol. 1811, no. 1, pp. 148–156, Jan. 2002.

[41] P. Mirchandani and L. Head, "A real-time traffic signal control system: Architecture, algorithms, and analysis," *Transp. Res. C, Emerg. Technol.*, vol. 9, no. 6, pp. 415–432, Dec. 2001.

[42] M. A. Wiering, "Multi-agent reinforcement learning for traffic light control," in *Proc. Mach. Learn., 7th Int. Conf. (ICML)*, 2000, pp. 1151–1158.

[43] E. Van Der Pol and F. A. Oliehoek, "Coordinated deep reinforcement learners for traffic light control," in *Proc. NIPS'16 Workshop Learn., Inference Control Multi-Agent Syst.*, 2016, pp. 1–8. [Online]. Available: https://www.fransoliehoek.net/docs/VanDerPol16LICMAS.pdf

[44] Z. C. Lipton, J. Berkowitz, and C. Elkan, "A critical review of recurrent neural networks for sequence learning," 2015, pp. 1–38, *arXiv:1506.00019*. [Online]. Available: https://arxiv.org/abs/1506.00019

[45] J. T. Lundgren and M. Patriksson, "An actor-critic algorithm for learning rate learning," *Signal Image Process., Int. J.*, vol. 3, no. 2003, pp. 29–39, 1976.

[46] J. Schulman, F. Wolski, P. Dhariwal, A. Radford, and O. Klimov, "Proximal policy optimization algorithms," 2017, *arXiv:1707.06347*. [Online]. Available: http://arxiv.org/abs/1707.06347

[47] S. Kakade and J. Langford, "Approximately optimal approximate reinforcement learning," in *Proc. ICML*, vol. 2, Jul. 2002, pp. 267–274.

[48] D. Krajzewicz, J. Erdmann, M. Behrisch, and L. Bieker, "Recent development and applications of SUMO-simulation of urban mobility," *Int. J. Adv. Syst. Meas.*, vol. 5, nos. 3–4, pp. 128–138, 2012.

[49] M. Abadi, P. Barham, J. Chen, Z. Chen, A. Davis, J. Dean, M. Devin, S. Ghemawat, G. Irving, and M. Isard, "TensorFlow: A system for large-scale machine learning," in *Proc. OSDI*, vol. 16, 2016, pp. 265–283.

[50] J. Glick. (2015). *Reinforcement Learning For Adaptive Traffic Signal Control*. [Online]. Available: https://github.com/JDGlick/sumo_reinforcement_learning

SHURONG LI received the B.S. degree in transportation and planning engineering from the Beijing Institute of Technology, China, in 2016. She is currently pursuing the Ph.D. degree with the MOT Key Laboratory of Transport Industry of Big Data Application Technologies for Comprehensive Transport, School of Traffic and Transportation, Beijing Jiaotong University, Beijing, China. Her current research interests include adaptive traffic signal control and automatic vehicle trajectory planning.

CHONG WEI received the M.S. and Ph.D. degrees from Kobe University, Kobe, Japan, in 2007 and 2009, respectively. He was appointed as the Ph.D. Supervisor, in 2015. He is currently an Associate Professor with the School of Traffic and Transportation, Beijing Jiaotong University, Beijing, China. His research areas include dynamic traffic network modeling, vehicle routing problem, and traffic flow theory. He also serves as the Editorial Board Member for multiple international journals, such as the *International Journal of Intelligent Traffic System* and the *International Journal of Transport*.

XUEDONG YAN received the Ph.D. degree in civil engineering from the University of Central Florida, Orlando, FL, USA. He is currently a Professor with the School of Traffic and Transportation, Beijing Jiaotong University, Beijing, China, where he is also the Executive Director of the MOT Key Laboratory of Transport Industry of Big Data Application Technologies for Comprehensive Transport and the Vice President. His research interests include traffic safety, driving simulation, urban planning, and management.

LU MA received the Ph.D. degree in civil engineering from the University of Florida. He is currently an Associate Professor with the School of Traffic and Transportation, Beijing Jiaotong University, Beijing, China. His research interests include intelligent transportation systems, transportation planning, traffic flow theory, and traffic accident analysis.

DEQI CHEN received the B.S. degree in transportation and planning engineering from Inner Mongolia University, China, in 2016. He is currently pursuing the Ph.D. degree with the MOT Key Laboratory of Transport Industry of Big Data Application Technologies for Comprehensive Transport, School of Traffic and Transportation, Beijing Jiaotong University, Beijing, China. His current research interests include data-driven short-term traffic prediction and intelligent transportation systems.

YING WANG received the B.S. degree from the School of Engineering and Technology, Northeast Forestry University, Harbin, China, in 2017. She is currently pursuing the Ph.D. degree with the MOT Key Laboratory of Transport Industry of Big Data Application Technologies for Comprehensive Transport, School of Traffic and Transportation, Beijing Jiaotong University, Beijing, China. Her research interest includes the trajectory planning of intelligent vehicles and nonlinear optimization.